Hamiltonian formalism for space charge dominated beams in a uniform focusing channel

A. Riabko, M. Ellison, X. Kang, S.Y. Lee, D. Li, J.Y. Liu, X. Pei, and L. Wang
Department of Physics, Indiana University, Bloomington, Indiana 47405
(Received 20 October 1994)

We employ the Kapchinskij-Vladimirskij envelope Hamiltonian [I. M. Kapchinskij and V. V. Vladimirskij, in *The Proceedings of the 9th International Conference on High Energy Accelerators*, edited by L. Kowarski (CERN, Geneva, 1959), p. 274] to describe the envelope evolution and the particle Hamiltonian to describe particle motion in a space charge dominated beam. Properties of the envelope function in a mismatched uniform focusing channel are studied. Parametric resonances of the particle Hamiltonian due to envelope oscillations of a mismatched beam are studied. We find that the Hamiltonian dynamics depends only on a single effective space charge parameter, the ratio of the space charge perveance to the focusing strength. The onset of global chaos exhibits a first order phase-transition-like behavior when the amplitude of envelope oscillations for a mismatched beam is larger than a critical value. This global chaos can greatly enhance the halo formation. The relation between the critical envelope mismatch for the halo formation and the effective space charge parameter is numerically obtained. Possible experiments are suggested.

PACS number(s): 07.77.−n, 29.27.Eg, 41.75.−i, 52.25.Wz

I. INTRODUCTION

The interest in intense charged particle beams has grown in the past few years due to the demand in high brightness and high intensity ion sources. The difficulties in transporting such a beam ranges from emittance blowup to halo formation. These problems can cause beam loss and radiation damage to the transport line [1,2].

For beams dominated by the self-space-charge force, Kapchinskij and Vladimirskij (KV) have constructed a self-consistent equilibrium distribution function, which obeys the KV equation governed by the external focusing force and the force due to self-beam charge and current [3]. Since this pioneering development, there have been many progresses on problems related to beam dynamics of the space charge dominated beams, such as the concept of rms emittance, the envelope equation, etc. [4,5]. When the KV envelope function, governed by the external focusing and the self-nonlinear electromagnetic force, experiences a time dependent modulation, nonlinear parametric resonances may play an important role in the envelope dynamics. In particular, nonlinear properties of the KV equation in a periodic focusing solenoidal field were extensively studied in Refs. [5,6].

In a similar spirit, the motion of beam particles obeys the Hill's equation, which takes into accounts the focusing force and the self-space-charge force. Thus the beam transport of a space charge dominated beam is modeled in a one-way "self-consistency" by studying simultaneously the KV and Hill's equations. This is usually achieved by numerical simulations. Results of numerical simulations have indicated that the halo formation arises mainly from resonance excitations [2,7–9]. On the other hand, experimental measurements and numerical simulations have been used to verify the theory that the emittance growth is related to nonlinear electric field energy [10–12]. In particular, Ref. [12] showed that the emittance of a proton beam grew very fast in a short distance of a transport channel without a focusing field.

Alternately, the Fokker-Planck equation has been used to describe the halo formation in a space charge dominated beam [13]. All of the complicated mechanisms such as mode-particle, mode-mode interactions and resonances are lumped into the dynamics of the Fokker-Planck-like equation. Energy conversion from the envelope mismatch to thermal energy was used to interpret the halo formation.

To achieve microscopic understanding of particle motion, we choose to study particle motion by solving the KV and Hill's equations, where numerical simulations have shown that chaos plays an important role in halo formation. Although numerical simulations are very useful in obtaining a visual chaos, they often lead to confusion when the number of parameters is large. Sometimes, it is difficult to understand the underlying physics based on numerical simulations alone. Furthermore, because correlations between parameters are usually nonlinear, the task of unravelling a key condition for halo formation is hindered by numerical chaos. Therefore, analytic analysis is useful. In this respect, Gluckstern has recently obtained an analytic solution for the second order resonance in a space charge dominated beam [14]. Our work furthers the goal of studying chaos generated by overlapping parametric resonances.

The beam transport model can be divided into two coupled oscillations, where the KV envelope Hamiltonian is used to describe the envelope oscillations [6], and the Hill's equation that includes the focusing and space charge forces is used to describe the betatron oscillations. Here, the assumption is that the envelope evolution will affect the particle motion, while the evolution of particle motion does not affect the envelope function. This is a

reasonable assumption, because the fraction of particles outside the envelope is small. The particle Hamiltonian that gives rise to the Hill's equation can then be expanded in the particle action-angle variables of an unperturbed particle Hamiltonian. Families of parametric resonances arises naturally from this procedure [15,16].

This simple theoretical model has the merit of understanding the essential physics analytically. Multiparticle simulations [9] and possible experiments can be used to verify this model. We organize this paper as follows. In Sec. II, we review properties of the envelope Hamiltonian and study the evolution of the envelope function for a mismatched beam in a uniform focusing channel. In Sec. III, the particle Hamiltonian of a space charge dominated beam is expanded in action-angle variables of an unperturbed Hamiltonian. We will show that parametric resonances can arise from the harmonic modulation of the space charge force due to a mismatched envelope function. The harmonic modulation produces coherent excitation to Hamiltonian tori. Dependence of the parametric resonances on the space charge parameter will be discussed. Conditions for global chaos and halo formation will be examined. Possible experiments for the observation of the enhanced halo formation resulting from global chaos will be discussed in Sec. IV, and the effects of angular momentum will be studied in Sec. V. Conclusions and discussions will be presented in Sec. VI.

II. THE HAMILTONIAN FOR THE ENVELOPE PHASE SPACE

Using the longitudinal distance s as the time coordinate, the KV Hamiltonian for a transport channel with paraxial symmetry is given by $H_e = \frac{1}{2}P_b^2 + \tilde{V}_{\rm KV}(R_b)$, where R_b is the equilibrium radius of the beam, (P_b, R_b) are the conjugate *envelope phase space* coordinates, and the KV potential is given by

$$\tilde{V}_{\rm KV} = \frac{1}{2}k_f(s)R_b^2 - K_b \ln R_b + \frac{\epsilon^2}{2R_b^2}. \tag{1}$$

Here $k_f(s)$ is the external focusing field, and ϵ is the emittance of the beam. The space charge perveance parameter of the beam is given by $K_b = \frac{2N r_{\rm cl}}{\beta^2\gamma^3}$, where $r_{\rm cl}$ is the classical radius of the particle, β and γ are the relativistic factors of the beam, and N is the number of particles per unit length. For a uniform focusing channel, $k_f(s)$ is constant. For a periodic focusing channel, $k_f(s)$ is periodic, i.e., $k_f(s) = k_f(s+L)$, where L stands for the cell length of the focusing field.

We transform the KV Hamiltonian to a dimensionless form [5] using the following dimensionless parameters and variables: $\theta = 2\pi\frac{s}{L}$ for the time variable, $k(\theta) = L^2 k_f(s)$ for the dimensionless focusing strength in a periodic cell, $K = \frac{LK_b}{\epsilon}$ for the space charge perveance parameter, and

$$R = \frac{R_b}{\sqrt{\epsilon L}}, \quad P = \sqrt{\frac{L}{\epsilon}}P_b \tag{2}$$

for the dimensionless envelope phase space coordinates. Here L is the basic period of the accelerator structure. The parameter $\frac{K}{4\pi} = \frac{LK_b}{4\pi\epsilon}$ signifies the linear space charge tune shift *á la* circular synchrotrons. For a uniform focusing channel with a matched envelope function, the basic period L is arbitrary. In this paper, we study only the uniform focusing channel, i.e., $k(\theta) = \mu^2$, where μ corresponds to the phase advance of transverse betatron oscillations. In terms of new phase space coordinates, the envelope Hamiltonian becomes

$$H_e = \frac{1}{4\pi}P^2 + \frac{1}{4\pi}\mu^2 R^2 - \frac{1}{2\pi}K\ln R + \frac{1}{4\pi R^2}. \tag{3}$$

We will show later (see Sec. IV) that the relevant focusing parameter in the uniform focusing channel is the phase advance per unit length $\mu_f = \mu/L$.

A. Envelope function in a uniform focusing channel

For a uniform focusing channel, the scaling factor L is arbitrary. The result will be independent of L used in the scaling transformation. The dimensionless equilibrium envelope radius for the matched beam is given by

$$R_0 = \left(\frac{1}{\mu}(\sqrt{\kappa^2+1}+\kappa)\right)^{1/2}, \tag{4}$$

where the effective space charge parameter,

$$\kappa = \frac{K}{2\mu}, \tag{5}$$

is the only scaling factor of the dynamical system (see Appendix A). Because the Hamiltonian in Eq. (3) is integrable, the envelope radius for a mismatched beam will follow an envelope torus of the Hamiltonian flow. The action of a given envelope torus is

$$J_e = \frac{1}{2\pi}\oint PdR = \frac{1}{\sqrt{\pi}}\oint[E_e - V_0(R)]^{1/2}dR, \tag{6}$$

where E_e is the "energy" of the envelope Hamiltonian given by

$$H_e = E_e(J_e) = \nu_e J_e + \tfrac{1}{2}\alpha_e J_e^2 + \cdots. \tag{7}$$

The tune of the Hamiltonian, defined as the number of oscillations in one period, is given by

$$Q_e(J) = \frac{dE_e}{dJ_e} = \nu_e + \alpha_e J_e + \cdots, \tag{8}$$

where the nonlinear detuning parameter,

$$\alpha_e = \frac{3}{64\pi^3 R_0^4 \nu_e^2}\left(K + \frac{10}{R_0^2}\right) - \frac{5}{384\pi^5 R_0^6 \nu_e^4}\left(K + \frac{6}{R_0^2}\right)^2 + \cdots, \tag{9}$$

can easily be obtained by the canonical perturbation method, and

$$\nu_e = 2\frac{\mu}{2\pi}\left[1 - \kappa\left(\sqrt{\kappa^2+1} - \kappa\right)\right]^{1/2} \tag{10}$$

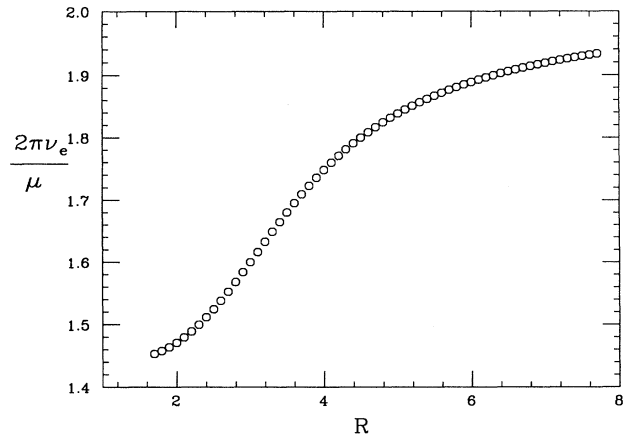

FIG. 1. The envelope tune Q_e normalized to $\frac{\mu}{2\pi}$ vs the maximum amplitude $R = \hat{R}$ for an envelope torus is shown for parameters $R_0 = 1.4199$ and $\kappa = 2.1913$. Note that the envelope tune depends quadratically on $\hat{R} - R_0$ for a small $\hat{R} - R_0$. Asymptotically, we have $2\pi Q_e/\mu \to 2$ as $R \to \infty$. For a space charge dominated beam with $K/2\mu \gg 1$, we have $2\pi Q_e/\mu \to \sqrt{2}$ as $R \to R_0$.

is the tune of small amplitude envelope oscillations. The phase advance of the envelope function in one period is 2μ at a zero space charge limit, and $\sqrt{2}\mu$ at the infinite space charge limit. For a linear system, one can intuitively see that the tune of the envelope function is twice the corresponding betatron tune, i.e., $\nu_e = 2(\frac{\mu}{2\pi})$, and independent of J_e. In the presence of the space charge force, the envelope tune will have the following asymptotic properties: $Q_e(J_e = 0) = \nu_e$ and $Q_e(J_e \to \infty) \to \frac{\mu}{\pi}$, i.e., $Q_e \in [\nu_e, \frac{\mu}{\pi})$. Therefore, the nonlinear detuning α_e arises solely from the space charge alone. Figure 1 shows a typical example of $\frac{2\pi Q_e}{\mu}$ as a function of the envelope amplitude for the parameters $R_0 = 1.4109$ and $\kappa = 2.1913$.

Using the generating function

$$F_2(R, J_e) = \int_{\hat{R}}^{R} P dR, \tag{11}$$

where $\hat{R}$ is the maximum amplitude of an envelope torus, the conjugate angle coordinate is given by

$$\psi_e = \frac{\partial F_2}{\partial J_e} = 2\pi \frac{\partial E_e}{\partial J_e} \int_{\hat{R}}^{R} \frac{dR}{P}. \tag{12}$$

Hamilton's equations motion are $\dot{J}_e = 0$, i.e., J_e is invariant, and $\dot{\psi}_e = Q_e(J)$, i.e., $\psi_e = Q_e(J)\theta + \psi_{e0}$.

B. Small amplitude envelope oscillations

For a weakly mismatched beam, we can expand the envelope function around the average radius, i.e., $R = R_0 + Y$. The resulting envelope Hamiltonian is given by

$$H_e \approx \frac{1}{4\pi} P^2 + \pi \nu_e^2 Y^2 + \cdots. \tag{13}$$

Thus the envelope function of a weakly mismatched beam is given by

$$R \approx R_0 + \left(\frac{J_e}{\pi\nu_e}\right)^{1/2} \cos \nu_e \theta, \tag{14}$$

where the action is given by $J_e \approx \pi\nu_e(\hat{R} - R_0)^2$ for small amplitude oscillations. Since the tune Q_e, shown in Fig. 1, depends quadratically on $\hat{R} - R_0$ up to about $\hat{R} \approx 3$, the expansion of Eq. (8) is a good approximation within the same range.

For later reference, we define a mismatch parameter M as

$$M = \frac{R_0 - R_{\min}}{R_0} = \frac{1}{R_0}\sqrt{\frac{J_e}{\pi\nu_e}}, \tag{15}$$

where $R_{\min}$ is the minimum of the envelope radius of a mismatched beam. This definition differs from that of Refs. [2,7,8], where they define $\tilde{M} = R_{\max}/R_0$ as the mismatch parameter, where $R_{\max}$ is the maximum envelope radius. In our definition, a matched beam has $M = 0$. Because of small anharmonicity in the envelope potential, the envelope oscillations may be nonsymmetric with respect to R_0. For example, when $\kappa = 2.5$, the radius of a beam with $M = 0.2$ will oscillate between $0.8R_0$ and $1.24R_0$.

III. THE HAMILTONIAN FOR THE PARTICLE PHASE SPACE

Using the longitudinal coordinate s as the time variable, the *particle Hamiltonian* for transverse oscillations in a paraxial symmetry transport channel is given by

$$H_p = \tfrac{1}{2}(p_x^2 + p_z^2) + \tilde{V}_p(x, z), \tag{16}$$

where (x, p_x, z, p_z) are transverse phase space coordinates in the Larmor precessing frame [1,5]. The transverse focusing potential $\tilde{V}_p(x, z)$ that includes self-fields of the beam in the KV model is given by

$$\tilde{V}_p = \frac{1}{2}k_f(s)r^2 - \frac{K_b}{2R_b^2}r^2\Theta(R_b - r) - \frac{K_b}{2}\left(1 + 2\ln\frac{r}{R_b}\right)\Theta(r - R_b), \tag{17}$$

where $r = \sqrt{x^2 + z^2}$. Using the generating function

$$F_2(x, z, p_r, p_\varphi) = p_r\sqrt{x^2 + z^2} + p_\varphi \arctan\frac{z}{x}, \tag{18}$$

where p_r and p_φ are new momenta with conjugate coordinates (r, φ), respectively, the rotationally symmetric Hamiltonian becomes

$$H_p = \frac{1}{2}\left(p_r^2 + \frac{p_\varphi^2}{r^2}\right) + \tilde{V}_p(r). \tag{19}$$

Since the Hamiltonian is independent of the angle variable φ, the momentum p_φ is invariant, which corresponds to the conservation of angular momentum [5,14]. The system reduces to a one-dimensional (1D) equation of motion. In this section, we will study a restricted 1D motion with $p_\varphi = 0$. The effects of a nonzero angular momentum will be discussed in Sec. V.

Using y_b to stand for either x or z coordinates, and p_b for either p_x or p_z, θ for the time variable, and the normalized coordinates of Eq. (2) with

$$y = \frac{y_b}{\sqrt{\epsilon L}}, \quad p = \sqrt{\frac{L}{\epsilon}} p_b, \tag{20}$$

for the conjugate phase space coordinates, the Hamiltonian becomes

$$H_p = \frac{1}{4\pi}p^2 + \frac{1}{4\pi}k(\theta)y^2 - \frac{K}{4\pi R^2}y^2\Theta(R-|y|) - \frac{K}{4\pi}\left(1 + 2\ln\frac{|y|}{R}\right)\Theta(|y|-R), \tag{21}$$

where R follows the KV Hamiltonian flow discussed in Sec. II, and Θ is the step function used to describe space charge potential inside or outside the core given by $\Theta(\zeta) = 1$ for $\zeta \geq 0$ and 0 otherwise. Hamilton's equations of motion for the beam in the uniform focusing channel are given by

$$\dot{y} = \frac{1}{2\pi}p, \tag{22}$$

$$\dot{p} = -\frac{1}{2\pi}\mu^2 y + \frac{K}{2\pi R^2}y\Theta(R-|y|) + \frac{1}{2\pi}\frac{K}{y}\Theta(|y|-R). \tag{23}$$

A scaling property of the envelope and particle Hamiltonians is discussed in Appendix A. If the envelope radius is constant, the Hamiltonian (21) is time independent and the energy is a constant of motion. However, if the envelope radius R depends on the time θ, the nonlinear system is not integrable.

For a weakly mismatched beam, the envelope function is given by Eq. (14), i.e., $R = R_0(1 - M\cos\nu_e\theta)$. Expanding the radius R about R_0, the particle Hamiltonian for a weakly mismatched beam is given by

$$H_p = H_{p0} + \Delta H_p. \tag{24}$$

The unperturbed Hamiltonian H_{p0} is given by

$$H_{p0} = \frac{1}{4\pi}p^2 + \frac{1}{4\pi}\mu^2 y^2 - \frac{K}{4\pi R_0^2}y^2\Theta(R_0-|y|) - \frac{K}{4\pi}\left[1 + 2\ln\frac{|y|}{R_0}\right]\Theta(|y|-R_0), \tag{25}$$

and the perturbation is obtained by expanding R around R_0 in Eq. (21) (see also Appendix B), i.e.,

$$\Delta H_p \approx -\frac{K}{2\pi R_0^2}\left[\frac{Y}{R_0}(y^2 - R_0^2) + \frac{3Y^2}{2R_0^2}(y^2 - \tfrac{1}{3}R_0^2) + \cdots\right] \times\Theta(R_0 - |y|), \tag{26}$$

where $Y = R_0 - R = MR_0\cos\nu_e\theta$. Note here that we have thrown away many time dependent terms, which do not depend on the phase space variables (y, p). These terms contribute to the fluctuation of Hamiltonian values without giving rise to resonance phenomena. Since the Coulomb force depends only on the total charge inside the envelope radius, the envelope oscillations do not perturb particle motion outside the envelope radius, and the perturbing potential exists only inside the envelope radius.

A. Action-angle variables of the unperturbed Hamiltonian

Due to a weakly mismatched beam envelope oscillations, particle motion experiences a time dependent modulation. To understand the effect of time dependent perturbation, we expand the perturbation in action-angle variables of the unperturbed Hamiltonian. The action for a torus of the unperturbed Hamiltonian is given by

$$J_y = \frac{1}{2\pi}\oint p\,dy. \tag{27}$$

The scale transformation of Eq. (20) transforms the actual action of a beam particle by the scaling factor of the emittance ϵ, i.e.,

$$J_b = \frac{1}{2\pi}\oint p_b dy_b = \epsilon J_y. \tag{28}$$

Using the generating function

$$F_2(y, J_y) = \int_{\hat{y}}^{y} p dy, \tag{29}$$

the conjugate angle variable is given by

$$\psi_y = \frac{\partial F_2}{\partial J_y} = 2\pi\frac{\partial E_p}{\partial J_y}\int_{\hat{y}}^{y}\frac{dy}{p}. \tag{30}$$

The energy of the unperturbed Hamiltonian is a function only of the action, i.e., $E_p(J_y)$. The particle tune is given by

$$Q_y(J_y) = \frac{\partial E_p}{\partial J_y}. \tag{31}$$

We will find in the next section that the power series expansion of the particle tune for a space charge dominated beam differs from that of Eq. (8).

1. Properties of the unperturbed particle Hamiltonian flow

For a beam with a matched space charge envelope, the beam radius is R_0. Particle motion, governed by the Hamiltonian (25), can be divided into three regions.

1. Particles inside the equilibrium KV envelope radius: Here we have $E_p \leq E_{p0}$ with $E_{p0} = \pi\nu_y^2 R_0^2 = \frac{1}{2}\nu_y$ and the betatron tune depression given by

$$\nu_y = \frac{\mu}{2\pi}[\sqrt{\kappa^2+1} - \kappa]. \tag{32}$$

Particle motion in this "energy" region is sinusoidal. The action is related to the energy by $E_p = \nu_y J_y$. Thus the tune of particle motion is constant, i.e., $Q_y = \nu_y$ with $\nu_y \sim \frac{\mu}{4\pi\kappa}$, when $\kappa \gg 1$. Since all particle motion inside the core has an identical tune ν_y, the space charge force causes a *constant incoherent* tune shift by $\Delta\nu_y = \frac{\mu}{2\pi} - \nu_y$. The particle motion can be described by

$$y = \sqrt{\frac{J_y}{\pi\nu_y}}\cos\nu_y\theta, \quad p = -\sqrt{4\pi\nu_y J_y}\sin\nu_y\theta. \tag{33}$$

The maximum action is given by $\hat{J}_y = \pi\nu_y R_0^2 = \frac{1}{2}$. This result is a trivial fact, by definition of Eq. (28), that the emittance ϵ of a matched beam is twice the maximum attainable action for particle motion in the original phase space. The torus for particles on the matched envelope ellipse is given by

$$\frac{y_e^2}{R_0^2} + R_0^2 p_e^2 = 1. \tag{34}$$

2. $E_p \to \infty$, $J_y \to \infty$: In the limit of a large action, the space charge force is not important. Thus we have $Q_y(J_y \to \infty) \to \frac{\mu}{2\pi}$.

3. $E_{p0} \le E < \infty$: $Q_y \in [\nu_y, \frac{\mu}{2\pi})$. The tune of a test particle outside the core lies within the range $[\nu_y, \frac{\mu}{2\pi})$.

In the infinite space charge limit with $K \to \infty$ while keeping $\epsilon K/L = K_b$ constant, we have $R_b = \sqrt{\epsilon L}R_0 = \sqrt{K_b}/\mu_f$ and $\nu_y \to 0$. Some properties of particle oscillations at a large κ just outside the envelope core are listed as follows:

$$\hat{y} \approx R_0 + \frac{\sqrt{2\pi(E_p - E_{p0})}}{\mu},$$

$$J_y \approx \frac{1}{2} + \frac{4R_0}{\sqrt{\pi}}(\sqrt{E_p} - \sqrt{E_{p0}}) + \frac{\sqrt{2\pi}}{\mu}(E_p - E_{p0}),$$

$$\frac{2\pi Q_y}{\mu} \approx \frac{2\pi\nu_y}{\mu} + \frac{\pi^2}{8\kappa}(J_y - \tfrac{1}{2}),$$

where we observe that the particle tune will show a cusp at the envelope action. The slope dQ_y/dJ_y is inversely proportional to κ. Some examples of normalized particle tunes $\frac{2\pi Q_y}{\mu}$ vs J_y are shown in Fig. 2 for parameters $(R_0, \kappa) = (1,1), (1.4199, 2.1913)$, and $(2.0, 5.0)$, respectively. The cusp of the particle tune shown in Fig. 2 indicates that a simple power series expansion may not be a good approximation for the exact particle tune of a space charge dominated beam. At the same time, the sharp rise of the particle tune near $\hat{J}_y = \frac{1}{2}$ will bear important implications to parametric resonances when the system is perturbed harmonically. Such a harmonic perturbation can be generated by wake fields of vacuum chamber impedances, or by the space charge force resulting from mismatched envelope oscillations. In this paper, we discuss only the latter perturbation.

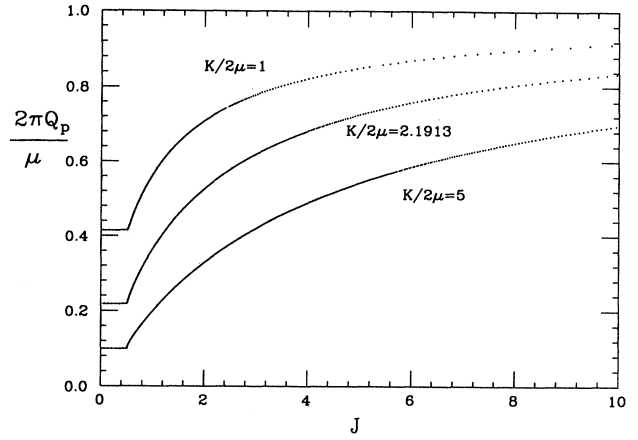

FIG. 2. The particle tune Q_y, normalized to $\frac{\mu}{2\pi}$, is plotted vs the particle action $J = J_y$ for $(R_0, \kappa) = (1,1), (1.4199, 2.1913), (2,5)$, respectively. Asymptotically, we have $\frac{2\pi Q_y}{\mu} \to 1$ as $J_y \to \infty$.

2. *The envelope torus of a weakly mismatched beam*

Although the Hamiltonian (24) is a good model (see Appendix B) for studying resonances in Eq. (21), we should bear in mind that the particle motion is governed by Hamilton's equations of motion (23), and we are studying a test particle under the influence of the mismatched envelope oscillations in the KV equilibrium equation. For a mismatched beam with particles distributed uniformly inside the envelope with an emittance ϵ, the envelope ellipse at the minimum beam envelope locations can be expressed as

$$\frac{y_e^2}{(1-M)^2 R_0^2} + (1-M)^2 R_0^2 p_e^2 = 1. \tag{35}$$

Within the model of the coupled KV and Hill's equations, particles initially inside the core will reside inside the core for all times, i.e., the modulation of the mismatched envelope function does not cause particles to leave the core. This can easily be proved by observing that the Hill's equation inside the core is linear. *Time dependent modulation to a linear system does not destroy tori* unless a linear Mathieu instability is encountered.

3. *Linear Mathieu instabilities*

For particle energy below E_{p0}, the Hamiltonian is linear. The equation of motion for a particle in a mismatched beam is given by

$$\ddot{y} + \left(\nu_y^2 + \frac{KM}{2\pi^2 R_0^2}\cos\nu_e\theta\right) y = 0. \tag{36}$$

This is the Mathieu's equation. The first order Mathieu's instability occurs when the condition

$$\frac{\nu_y}{\nu_e} \in \left(\frac{1}{2} - \frac{KM}{4\pi^2\nu_e^2 R_0^2}, \frac{1}{2} + \frac{KM}{4\pi^2\nu_e^2 R_0^2}\right) \tag{37}$$

is satisfied. This is equivalent to the half integer stopband in circular synchrotrons, where ν_e serves as the revolution tune and ν_y plays the role of the betatron tune. However, we will see later (Sec. III B 1) that the *linear* Mathieu instability is *not* important to particle motion in a space charge dominated beam.

B. Parametric resonances

Now the task is to expand the perturbation in action-angle variables of the unperturbed Hamiltonian. For example, the term linear in M can be obtained with

$$(y^2 - R_0^2)\Theta(R_0 - y) = \sum_{n=-\infty}^{\infty} G_n(J_y) e^{in\psi_y}, \tag{38}$$

where

$$G_n(J_y) = \frac{1}{2\pi}\int_{-\pi}^{\pi} (y^2 - R_0^2)\Theta(R_0 - y) e^{-in\psi_y} d\psi_y, \tag{39}$$

with $G_{-n} = G_n^*$ and γ_n is the phase of G_n. Because the Hamiltonian of Eq. (24) is symmetric with respect to $y \to -y$, all odd harmonics vanish, i.e., $G_n = 0$ for $n =$ odd. The Hamiltonian can then be expressed as

$$H_p = E_p(J_y) + \frac{K}{4\pi R_0^2}\sum_{m=1}^{\infty}\sum_{n>0}^{\infty}(m+1)M^m|G_{n,m}| \times [\cos(n\psi_y - m\nu_e\theta + \gamma_n) + \cos(n\psi_y + m\nu_e\theta + \gamma_n)] + \cdots, \tag{40}$$

where $G_{n,1} = G_n$ of Eq. (39). Here only terms that are important to particle dynamics are explicitly shown. Terms with $m > 1$ are usually not important for a weakly mismatched beam. The resonance strength function $G_{n,m}$ can be obtained similar to that of Eq. (39) by replacing proper integrand, e.g., $(3y^2 - R_0^2)/2$ for $m = 2$, etc.

The Hamiltonian of Eq. (40) expressed in action-angle variables exhibits clearly parametric resonances. A coherent perturbation to a Hamiltonian torus occurs when the stationary phase condition, $n\dot{\psi}_y \approx m\nu_e$, is satisfied. Such a resonance is called a n:m primary resonance. To understand the effect of a resonance condition on the Hamiltonian flow, we perform another canonical transformation to the resonance rotating frame using the generating function

$$F_2 = \left(\psi_y - \frac{m}{n}\nu_e\theta + \frac{\gamma_n}{n}\right) I_y. \tag{41}$$

Here $I_y = J_y$ and $\phi_y = \psi_y - \frac{m}{n}\nu_e\theta + \frac{\gamma_n}{n}$ are conjugate phase space variables. Neglecting the time dependent terms, which are averaged to zero, we obtain the time averaged Hamiltonian in the resonance rotating frame as

$$\langle \tilde{H}_p \rangle \approx E_p(I_y) - \frac{m}{n}\nu_e I_y + h_{n,m}(I_y)\cos n\phi_y, \tag{42}$$

where the effective resonance strength $h_{n,m}$ is given by

$$h_{n,m} = \frac{(m+1)M^m K}{4\pi R_0^2}|G_{n,m}(I_y)|. \tag{43}$$

The fixed points of the time averaged Hamiltonian is given by $\sin n\phi_{p,\mathrm{FP}} = 0$, and

$$nQ_y(I_{p,\mathrm{FP}}) - m\nu_e \pm nh'_{n,m}(I_{p,\mathrm{FP}}) = 0, \tag{44}$$

where the prime corresponds to the derivative with respect to I. There are thus n unstable fixed points (UFP's) and n stable fixed points (SFP's) in the particle phase space for the n:m resonance.

In particular, the Mathieu's resonance discussed in Sec. III A 3 is equivalent to the $n = 2, m = 1$ parametric resonance, where the origin of the particle phase space becomes unstable, i.e., $I_{p,\mathrm{UFP}} = 0$. This occurs when the condition

$$\frac{\nu_y}{\nu_e} \in \left(\frac{1}{2} - \frac{h'_{2,1}}{\nu_e}, \frac{1}{2} + \frac{h'_{2,1}}{\nu_e}\right) \tag{45}$$

is satisfied. This condition is equivalent to the Mathieu instability of Sec. III A 3.

1. *Parametric resonance conditions*

We would like to investigate the parametric resonance before the resonance strength calculation. Roughly speaking with the condition that $h'_{n,m} \approx 0$, the n:m resonance of Eq. (44) is approximately given by $Q_y/\nu_e \approx m/n$, where $Q_y/\nu_e \in [\frac{\nu_y}{\nu_e}, \frac{\mu}{2\pi\nu_e})$. Since ν_y/ν_e and $\mu/2\pi\nu_e$ depend only on the effective space charge parameter κ, the n:m parametric resonance condition depends only on κ. Figure 3 shows ν_y/ν_e and $\mu/2\pi\nu_e$ as a function of the parameter κ as solid curves, where the lower curve, for ν_y/ν_e, is the tune of particles inside the KV envelope with $J_y \in [0, \frac{1}{2}]$, the upper curve, for $\frac{\mu}{2\pi\nu_e}$, depicts the limit that $J_y \to \infty$, and the shaded region corresponds to particles with action $J_y \in (\frac{1}{2}, \infty)$. Horizontal lines, $\frac{1}{2}, \frac{1}{4}, \frac{1}{6}, \ldots$ corresponds to 2:1, 4:1, 6:1,... resonances.

Here we note that the 2:1 resonance condition is satisfied for all values of κ. This 2:1 resonance bifurcates at $J_y \le 1/2$ as $\kappa \to 0$, which becomes the linear Mathieu instability. Since the linear Mathieu's instability occurs only in the limit of zero space charge parameter, where the resonance strength is zero, it is *not* important. Using results of Sec. III A 1, the stable fixed point for the 2:1 resonance can be estimated to be $R_{\mathrm{SFP}} \sim 1.8R_0$ for large κ.

The fourth and the sixth order resonances bifurcate at $\kappa \approx \frac{3}{\sqrt{7}}$ and $\kappa \approx \frac{8}{\sqrt{17}}$, respectively. In general, the n:1 resonance can exist only at

$$\kappa \ge \frac{n^2 - 4}{\sqrt{8(n^2 - 2)}}. \tag{46}$$

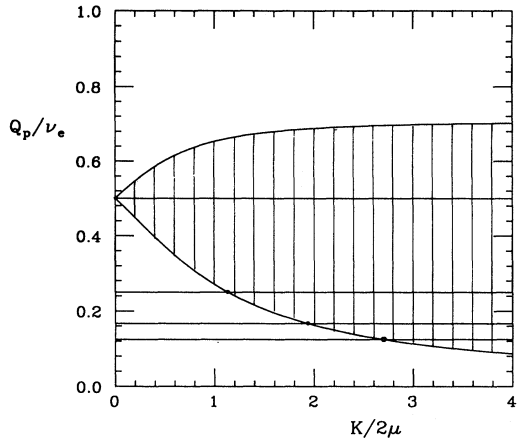

FIG. 3. The ratio of the particle tune to the envelope tune is plotted as a function of the effective space charge strength κ. The shaded region corresponds to the allowable region of the particle tune. Horizontal lines mark parametric resonances due to the envelope modulation. Note here that the 2:1 resonance can exist at all values of the effective space charge parameter. A higher order resonance exists only when the horizontal line intersects the shaded area.

The condition for the n:m resonance can be obtained by replacing n with $\frac{n}{m}$ in the above equation, e.g., the 8:3 resonance bifurcates at $\kappa = 0.4865$ and the 6:2 resonance bifurcates at $\kappa = 0.6682$. Although the higher order parametric resonance strength functions become zero at the envelope radius (see next section), particles near the envelope core can percolate into these resonance islands in numerical particle-in-cell calculations. In a real beam, particles can become more sensitive to errors and noise when parametric resonances are located just outside the envelope core.

Figure 4 shows Q_y/ν_e vs J_y for $\kappa = 2.1913$ (see the middle curve of Fig. 2). Here horizontal lines mark the

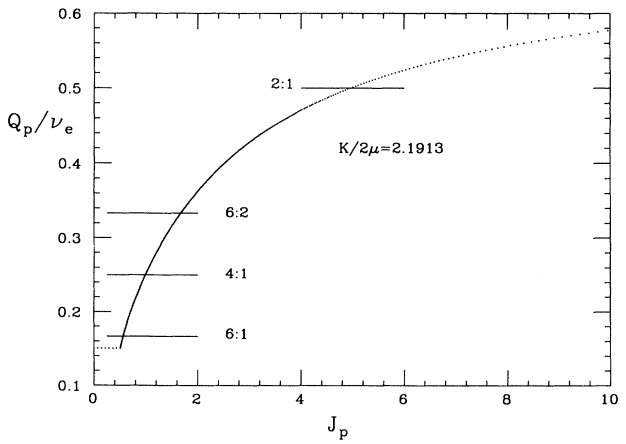

FIG. 4. Q_y/ν_e vs $J_p = J_y$ for the case with $\kappa = 2.1913$. Intersections of Q_y/ν_e with horizontal lines mark the fixed point locations of parametric resonances.

occurrence of the parametric resonance condition. It is worth noting that the 2:1 resonance is always further apart from high order resonances. This has important implications on the halo formation to be discussed later, where *halo particles are defined as beam particles which orbit about 2:1 resonance islands.* In fact, as the parameter κ increases, the fixed point of the 2:1 resonance moves away from the core with $J_{\mathrm{FP};2:1} \sim (\sqrt{\kappa^2+1}+\kappa)$. This process makes the core less susceptible to the halo formation. In reality, the radial extension of a beam with a large κ will be correspondingly larger, thus the halo formation will depend on the actual particle distribution in the tail region. The intersection of the horizontal line m/n with Q_y/ν_e curve in Fig. 4 corresponds to the n:m resonance action, $J_{\mathrm{FP};n:m}$. Based on our numerical simulations, we find a scaling property with

$$J_{\mathrm{FP};n:m}(\kappa) \approx C_{n:m}\kappa, \tag{47}$$

where $C_{2:1} \approx 2.15, C_{4:1} \approx 0.43, C_{6:1} \approx 0.24, \ldots$. This means that all resonances in this dynamical system expand almost uniformly as a function of the parameter κ.

2. The resonance strength

Since the equation of motion is linear for $y \le R_0$, the resonance strength of Eq. (39) can be obtained easily. First, for a particle inside the envelope, i.e., $E_p \le E_{p0} = \nu_y/2$ or $J_y \le 1/2$, the resonance strength is given by

$$G_n(J_y) = \frac{1}{4\pi\nu_y} J_y \delta_{n,2}, \tag{48}$$

where $\delta_{n,2}$ is the Kronecker δ function. This means that only the 2:1 resonance is possible inside the core. However, the resonance condition of Eq. (44) can reach the core only when $\kappa = 0$. Thus the Mathieu resonance is not important.

For a particle with energy E_p larger than E_{p0}, the resonance strength can also be obtained easily using Eq. (30), i.e.,

$$\begin{aligned} G_n = {} & \frac{(-)^{\frac{n}{2}}}{n\pi^2\nu_y^2}(E_p - 2E_{p0}) \sin\left(\frac{n}{2\nu_y}\frac{\partial E_p}{\partial J_y}\arcsin\sqrt{\frac{E_{p0}}{E_p}}\right) \\ & + \frac{(-)^{\frac{n}{2}+1}E_p}{2\pi^2\nu_y^2}\frac{\partial E_p}{\partial J_y} \\ & \times \left[\frac{\sin\left[\left(\frac{n}{\nu_y}\frac{\partial E_p}{\partial J_y}+2\right)\arcsin\sqrt{\frac{E_{p0}}{E_p}}\right]}{n\frac{\partial E_p}{\partial J_y}+2\nu_y}\right. \\ & \left. + \frac{\sin\left[\left(\frac{n}{\nu_y}\frac{\partial E_p}{\partial J_y}-2\right)\arcsin\sqrt{\frac{E_{p0}}{E_p}}\right]}{n\frac{\partial E_p}{\partial J_y}-2\nu_y}\right]. \end{aligned} \tag{49}$$

Figure 5 shows the resonance strength for $n = 2, 4, 6$ vs J_y for $\kappa = 1$ with $\mu = 2.4142$. It is worth noting that the $G_2(J_y > 1/2)$ is nearly constant. Because the resonance strength increases with κ, secondary resonances obtained by combining nearby primary resonances can become important for large κ [15].

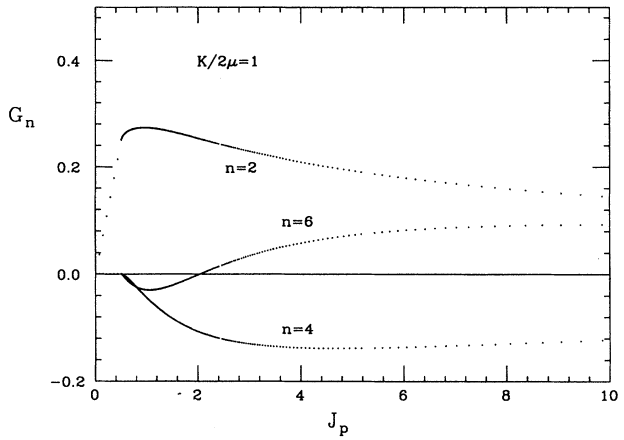

FIG. 5. The resonance strengths G_n for $n = 2, 4, 6$ are shown as a function of the particle action $J_p = J_y$ for $(\mu, K) = (2.5, 10)$.

3. *Numerical simulations*

To verify the parametric resonance condition discussed in earlier sections, numerical simulations are performed. Since the envelope function oscillates periodically, test particles experience periodic perturbation of the mean electric and magnetic forces. To eliminate the artificial time dependence of periodic modulation, hereafter, we examine only particle motion in Poincaré surfaces of section at the minimum envelope radius locations (see Appendix C). Figure 6 shows Poincaré surfaces of section for $\kappa = 1.501$ and $M = 0.2$, where the upper plot shows dominant 2:1, 4:1, and weak 6:2 resonances, and the lower plot shows a closeup view of the core region. We observe no other high order resonance in this case.

Increasing the space charge parameter κ, the resonance strength will be proportionally increased. More importantly, many more parametric resonances appear in the phase space. Figure 7 shows the Poincaré surfaces of section for $\kappa = 2.5$ with $M = 0.15$. In the upper plot, we find clearly 2:1, 8:3, and 4:1 resonances, while the 6:2 resonance is not explicitly visible due to the choice of initial condition. Note particularly that there is no higher order resonance than the 6:1 resonance in the lower plot.

There are two effects related to the mismatched parameter M. First, the envelope tune Q_e of Eq. (8) increases with the amplitude of envelope oscillations. Thus the shaded area of Fig. 3 is lowered. The condition for higher order resonances can be satisfied at a lower effective space charge parameter κ. However, this effect is small for a weakly mismatched beam. More importantly, the resonance strength increases with M and the secondary resonance may become more important by combining primary resonances. Figure 8 shows the Poincaré surfaces of section near the core for $\kappa = 2.5$ with $M = 0.2$. We note that there is no primary resonance beyond the 6:1 resonance. However, many secondary and tertiary resonances appear.

For a beam with a very large space charge parameter, many primary and secondary resonances appear near the core. The upper and the lower plots of Fig. 9 show the Poincaré surfaces of section near the core for $\kappa = 5$ with

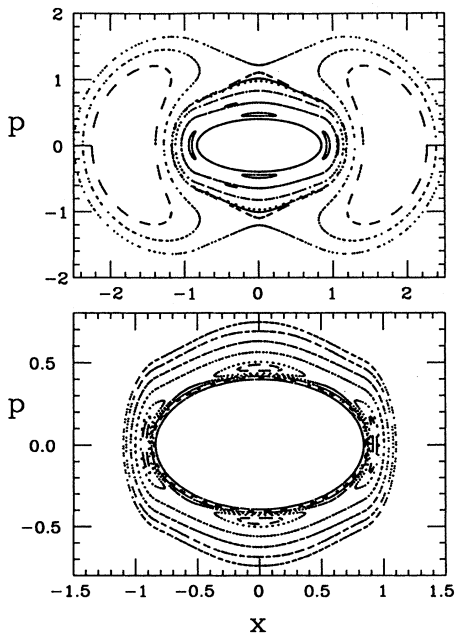

FIG. 6. Poincaré surfaces of section in particle phase space (x, p), where $x = y$, with parameters $M = 0.2$ and $(R_0, \kappa) = (1.049, 1.501)$. The lower plot is the closeup view of phase space maps near the core. See Appendix C for further explanation.

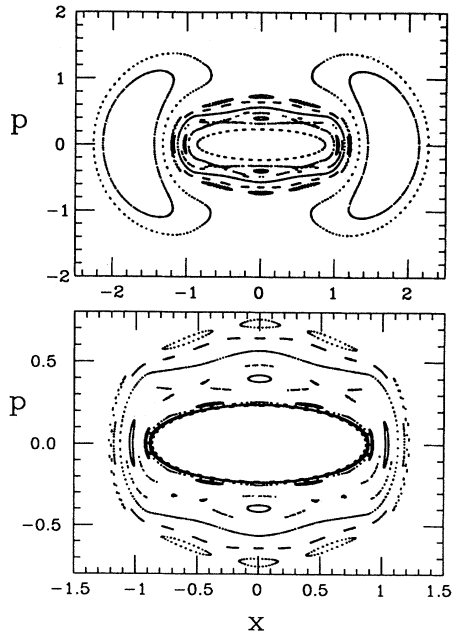

FIG. 7. Poincaré surfaces of section in particle phase space (x, p), where $x = y$, for a mismatch factor of $M = 0.15$ with parameters $(R_0, K) = (1.019, 2.5)$. The lower plot is a closeup view of the phase space near the core. See Appendix C for further explanation.

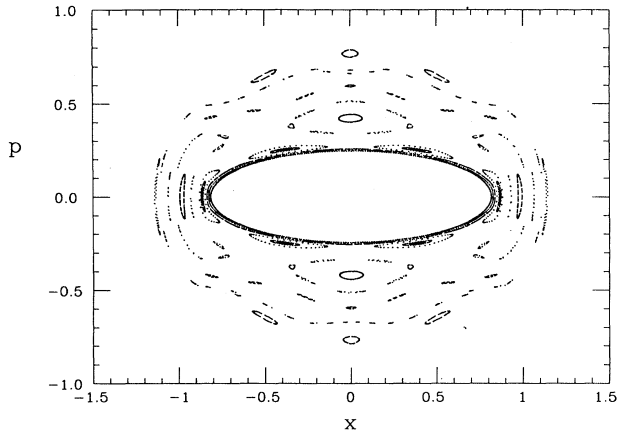

FIG. 8. The Poincaré surfaces of section in particle phase space (x,p), where $x=y$, for $(R_0,K)=(1.019,2.5)$ with the mismatch parameter $M=0.2$ near the core being enlarged to display many secondary and tertiary resonances (see also Fig. 7). See Appendix C for further explanation.

$M=0.1$ and 0.15, respectively. The 2:1 resonance, not shown in this figure, is located at $R_{\mathrm{SFP},2:1}\approx 1.8R_0$ similar to those of Figs. 6 and 7. With a small mismatch parameter $M=0.1$ shown in the upper plot, we observe 4:1, 8:1, 10:1 and 12:1 resonances. When the mismatch parameter is increased to 0.15 shown in the lower plot, local chaos becomes the essential feature in the phase space

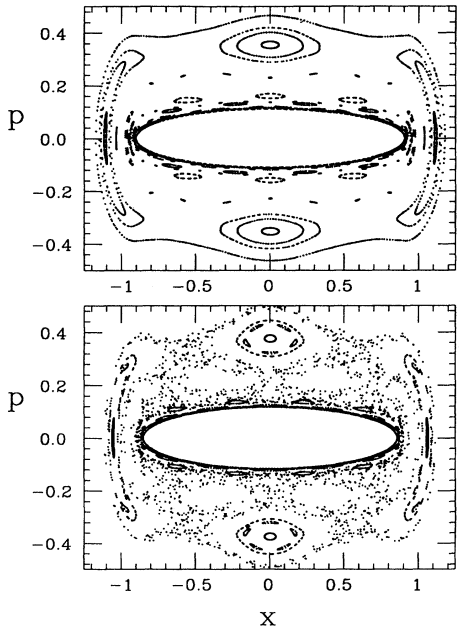

FIG. 9. Poincaré surfaces of section in particle phase space (x,p), where $x=y$, for $(R_0,K)=(1.005,5)$ with $M=0.1$ and 0.15 shown in the upper and lower plots, respectively. Note that local chaos becomes a dominant feature in the lower plot. See Appendix C for further explanation.

map. Because there is a torus, which separates the local chaos from the 2:1 resonance islands, this local chaos can enhance emittance growth without inducing halo formation provided that the beam distribution is within the boundary of the confinement torus.

C. Halo formation and global chaos

Within the KV model, all particles with actions less than 1/2 will remain inside the envelope function for a matched or mismatched beam. A mismatched envelope oscillates at the tune of Q_e and all particles inside the envelope oscillate at a tune of ν_y. *Since the core envelope remains intact and the motion of particles inside the envelope is linear, Hamiltonian tori inside the envelope can be distorted but not destroyed.* The only possible resonance inside the envelope is the linear Mathieu resonance, which is not important (see Sec. III B 1). The torus, which follows envelope oscillations with an action $J_y=\frac{1}{2}$, is called the envelope torus.

The Hamiltonian flow outside the envelope torus has a very different structure. The 2:1 resonance exists for all values of κ. The SFP and UFP of the 2:1 resonance are always outside the envelope torus. When the parameter κ increases, we find that the SFP action of 2:1 resonance is approximately given by $J_{\mathrm{FP},2:1}\approx\sqrt{\kappa^2+1}+\kappa$.

Since the envelope torus does not corrupt, how can halo be generated? The answer lies in the fact that particle distribution of finite temperature has a diffusive tail. When global stochasticity develops, particles outside the artificial KV envelope can become halo particles. *The diffusion process produces tail distribution and the resonance generates halo.* With this physical picture in mind, we investigate the dependence of the critical mismatch parameter M_c, which is defined as the envelope mismatch for the onset of global chaos, on the effective space charge parameter κ.

1. Poincaré energy

We consider a mismatched envelope ellipse given initially by Eq. (35). The evolution of the envelope ellipse is given by

$$\frac{y_e^2}{R^2(\theta)}+R^2(\theta)p_e^2=1, \tag{50}$$

where $R(\theta)$ describes the envelope oscillations in the transport channel. The Hamiltonian value (energy) of an envelope particle oscillates with time, but the action, $J_{ye}=\frac{1}{2}$, and the Poincaré surface of section are invariant. Since we always consider the Poincaré surfaces of section at the minimum radius locations [17], the maximum energy at $y_e=0$ is defined as the Poincaré energy for an envelope particle given by

$$E_{p,P}=\frac{1}{4\pi(1-M)^2R_0^2}=\frac{\nu_y}{2(1-M)^2}. \tag{51}$$

The Poincaré energy of a test particle outside the en-

velope ellipse is larger than $E_{p,P}$. We now consider the motion of a test particle outside the core with Poincaré energy $E_t = \eta E_{p,P}$ with $\eta > 1$. For a given mismatch parameter M, there is a critical number η_c such that all test particles with $\eta > \eta_c$ will orbit about the 2:1 resonance islands and become halo particles. Although particles with $\eta < \eta_c$ may encounter local chaos due to higher order primary or secondary resonances, they are bounded by a Hamiltonian torus, which separate the 2:1 resonance from the rest of the higher order resonances. Since higher order resonances usually stay close to the core, local chaos may enhance emittance dilution without generating halo provided that the initial beam distribution does not extend very far from the core. The lower plot of Fig. 9 is a clear example of the bounded local chaos. Here, a 10% tail distribution within the bounded local chaotic region can produce a factor of 2 increase in emittance.

2. *Halo and global chaos*

Figure 10 shows the η_c vs the mismatch parameter M for $\kappa = 2$ and 2.5, respectively. Here, a unique feature is a relatively "smooth dependence" of η_c vs M for $\kappa = 2$ and a "first order phase-transition-like" character for $\kappa = 2.5$. Numerical simulations indicate that a sharp transition in η_c occurs always when $\kappa \geq 2.2$. The critical mismatch parameter M_c can then be defined as the mismatched parameter where a sudden jump of the critical Poincaré energy occurs as shown on Fig. 10 reaching the envelope core, where $\eta_c \approx 1$. For example $M_c \approx 0.2975 \pm 0.0025$ at $\kappa = 2.5$. The physics of this sharp transition can be understood as follows.

When κ is small, there are few resonances near the core (see Figs. 3 and 4). Since the width of the 2:1 parametric resonance, or equivalently the corresponding Melnikov integral, varies smoothly with the parameter M, η_c will decrease smoothly as the parameter M increases. Along with the smooth decrease in η_c, a small stepwise decrease is expected arising from the overlapping 2:1 resonance with high order resonances one by one like a staircase. This is the case for $\kappa = 2$, shown as open circles in Fig. 10. Because there are relatively few resonances in the vicinity of the core, a small stepwise decrement in η_c appears when the 2:1 resonance overlaps with the 4:1 resonance around $M \approx 0.3$. The chaotic region produced by the overlapping 2:1 and 4:1 resonances is still relatively far away from the core. Therefore, η_c continues to decrease smoothly with respect to an increasing mismatch parameter M.

When κ is large, there are many primary and secondary resonances near the envelope core. This appears to be the case when $\kappa \geq 2.2$. As the mismatch parameter is varied, local chaos is formed near the envelope core for a small mismatch parameter. Once the stochastic layer of the 2:1 resonance overlaps with the boundary of the local chaos, mainly the 4:1 resonance, global chaos occurs. A sudden jump in the critical Poincaré energy shown in Fig. 10 for $\kappa = 2.5$ provides us a sensitive determination of the critical mismatch parameter M_c.

The top plot of Fig. 11 shows the critical mismatch parameter M_c as a function of the effective space charge parameter κ. We note that the critical M_c parameter is

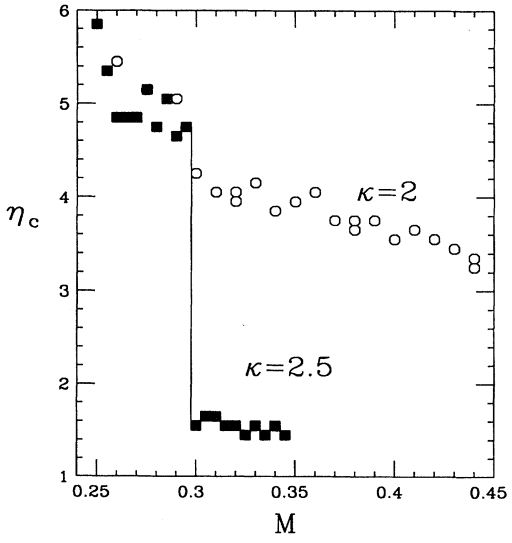

FIG. 10. The minimum Poincaré energy of a test particle that orbits the 2:1 resonance is shown as a function of the mismatch parameter for $\kappa = 2$ and 2.5, respectively. The critical mismatch parameter corresponds to the sudden jump of the Poincaré energies. In this example, $M_c \approx 0.2975$. Note that the smooth transition of the minimum Poincaré energy shown for $\kappa = 2$ has become a first order phase-transition-like behavior shown for $\kappa = 2.5$.

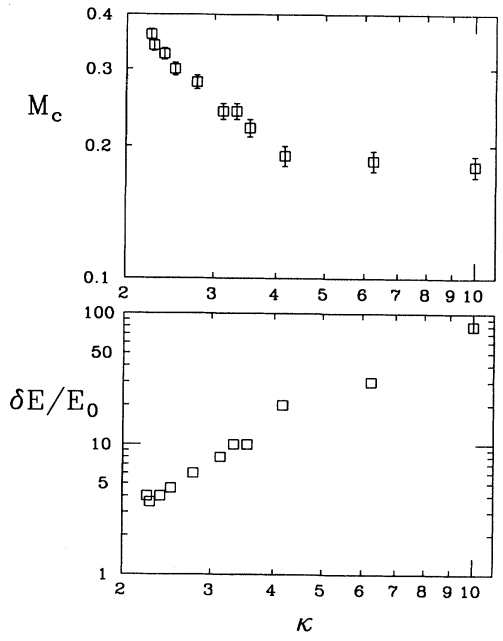

FIG. 11. The lower plot shows the gap of the Poincaré energy at the onset of global chaos. The dependence of the M_c vs the space charge parameter κ obtained from numerical simulations is shown in the upper plot.

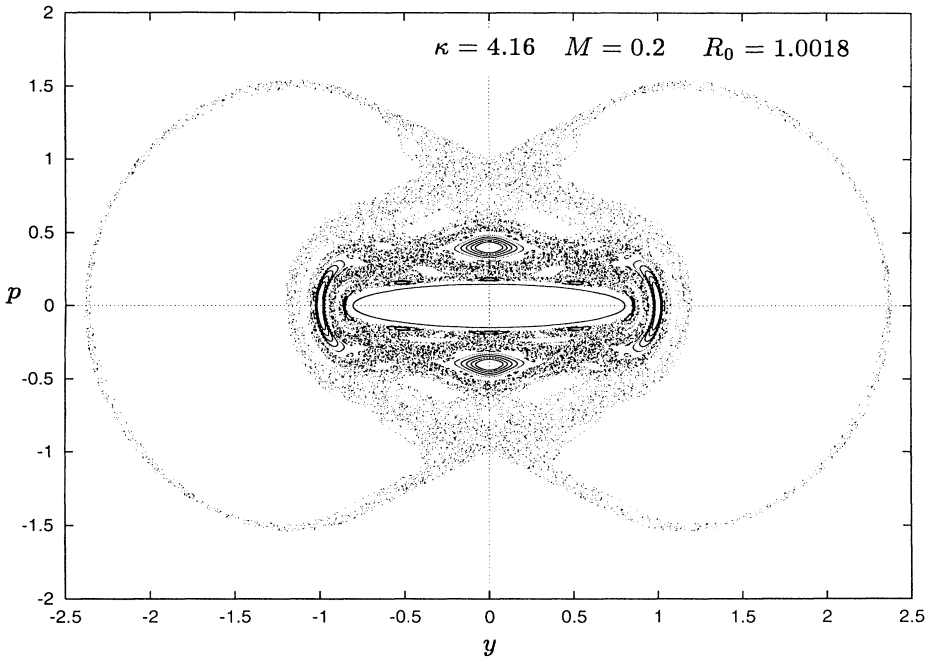

FIG. 12. The Poincaré surfaces of section at a global chaos condition with $\kappa = 4.16$ and $M = 0.2$. See Appendix C for further explanation.

almost constant when $\kappa > 4$. For $\kappa < 4$, the M_c vs κ can be fitted by either exponential form or power law. Unfortunately, it is difficult to derive the dependence of M_c on κ.

To verify that the sudden jump in the critical Poincaré energy is related to global chaos, we plot the change of the critical Poincaré energy $\delta E/E_0$ at $M = M_c$, where $E_0 = E_{p,P}$ is the Poincaré energy of the envelope, as a function of κ in the lower plot of Fig. 11. Since $E_0 \sim 1/\kappa$ shown in Eq. (51) and $\delta E/E_0 \sim \kappa^2$ shown in the lower plot of Fig. 11, we find that the critical transition jumps correspond to an energy gap between the stochastic layer of the 2:1 resonance and an orbit near the envelope core. This means that local chaos near the envelope torus has already developed. When $M > M_c$, all the phase space area between the 2:1 fixed point and the vicinity of the core is in chaos. The sudden phase transition is, therefore, related to the occurrence of global chaos where the separatrix of the 2:1 resonance overlaps with local chaos of higher order resonances near the core. An example of global chaos for the Poincaré surfaces of section is shown in Fig. 12 with parameters $\kappa = 4.16, M = 0.2$.

IV. SUGGESTED EXPERIMENTAL TESTS

Extensive numerical simulations on the space charge effects in circular synchrotrons have been performed [18]. Emittance growth has been observed to follow similar behavior as that of a space charge dominated transport line [10]. However, the space charge parameter κ for low energy beams in synchrotrons is typically $\kappa \approx 0.1$. The emittance growth in synchrotrons arises mainly from structure resonances.

The situation is different for the beam transport from an intense ion source. Typically, the rms normalized emittance of a proton or H^- beam of 30 mA at 35 KeV is about 0.1–0.2π mm mrad. The beam size is typically about 4 mm [19]. The space charge perveance for this beam will be about $K_b = 2.0 \times 10^{-3}$. Thus the matched focusing strength per unit length for this beam is about 11 m^{-1}. The resulting effective space charge parameter κ is about eight. Thus, particles outside the envelope function of such a beam may encounter many resonances if the beam envelope is not matched. The resonance condition depends only on the parameter κ alone while the beam radius depends on both μ and K parameters. In the above example, global chaos can result from a mistuned focusing channel with a focusing strength larger than 13.5 m^{-1} or less than 9.5 m^{-1}.

A. Time scale, matched beam size, and focusing strength

Before we look into possible experimental tests, we first examine the time scale. A space charge dominated beam has typically $N \sim 5 \times 10^{10}$ protons/meter. Assuming a 5-mm beam radius, we expect that the particle density is about $n \sim 10^{15}$ m^{-3}.

For a source of a given emittance, the match beam envelope is given by $R_b = \sqrt{\epsilon L} R_0$, where L is the scaling length. The matched focusing strength is given by

$$\mu_f = \frac{\sqrt{\epsilon^2 + K_b R_b^2}}{R_b^2}, \tag{52}$$

where $\mu_f = \frac{\mu}{L}$ is the betatron phase advance per unit length. Thus, once ϵ, K_b, and R_b are given, the matched focusing field μ_f is completely determined. Since $\epsilon^2 \ll$

$K_b R_b^2$ for a space charge dominated beam, we obtain $\mu_f \approx \sqrt{K_b}/R_b = \sqrt{2\pi n r_0}/(\beta\gamma^{3/2})$. Since the plasma frequency of the beam is given by $\omega_{pl} = \sqrt{4\pi n r_0 c^2}$, the distance that the particle travels in one plasma oscillation is given by

$$\lambda_{pl} = 2\pi\beta c/\omega_{pl} = \frac{\sqrt{2}\pi}{\sqrt{\gamma^3}\mu_f} \sim \frac{L}{\nu_e}. \tag{53}$$

Thus the plasma oscillation length of the beam particle is about the same as the length of the envelope oscillations.

Now, we examine characteristics of the 2:1 resonance. Following Eq. (42), the Hamiltonian for the 2:1 resonance can be expressed as

$$H_{2:1} \approx \frac{1}{2}\alpha_y (I - I_r)^2 + \frac{MK}{8\pi}\cos 2\phi_y, \tag{54}$$

where we have used the relation, $2\pi\nu_y R_0^2 = 1$ and $|G_2| \approx 1/8\pi\nu_y$. Our numerical simulations indicate that $\alpha_y\kappa \approx \frac{1}{3}\nu_e$. The characteristic tune of the 2:1 resonance becomes

$$\nu_{2:1} = \sqrt{\frac{\alpha_y \kappa M}{\nu_e}\frac{2\mu\nu_e}{2\pi}} \approx \sqrt{\frac{M}{3}}\left[1 - \frac{\kappa}{\sqrt{\kappa^2+1}+\kappa}\right]^{-1/4}\nu_e. \tag{55}$$

The width of the 2:1 resonance is approximately given by

$$\Delta I_{2:1} \approx 2\sqrt{3M}\left[1 - \frac{\kappa}{\sqrt{\kappa^2+1}+\kappa}\right]^{-1/4}\kappa. \tag{56}$$

Note here that the width of the 2:1 resonance is also proportional to κ.

A weakly mismatched beam at $M = 0.1 - 0.2$, the characteristic tune of the 2:1 resonance is about 0.1–0.2 of the envelope tune or the plasma oscillation tune. This means that a freshly scrapped beam with particles at the tail region of phase space will develop a complete halo in about 5–10 plasma oscillations.

B. Possible observations

Since the beam current depends on the extraction electric potential according to the Child's law, the beam intensity can be varied. Thus, a possible space charge beam transport experiment is to increase the beam intensity without changing the focusing strength. In this case, the space charge parameter κ and the mismatch parameter are both increased. Transport of this beam may encounter a threshold current for halo formation. Measurements of the threshold beam current can be used to verify the theoretical model for linking the onset of halo to the overlapping parametric resonances.

Another experimental test is to vary only the mismatch parameter. Assuming that the source emittance is constant, the effective space charge parameter can be kept constant by setting the phase advance per unit length μ_f proportional to the source intensity. However the matched beam radius is given by

$$R_b = \left(\sqrt{K_b^2 + 4\mu_f^2\epsilon^2} + K_b^2\right)^{1/2}/\sqrt{2}\mu_f. \tag{57}$$

If the beam source radius is constant, then the beam mismatch parameter is given by

$$M = \frac{|R_{\text{source}} - R_b|}{R_b}. \tag{58}$$

Measurements of the threshold mismatched parameter as a function of the space charge parameter can be used to verify the onset of global chaos shown in Fig. 10. This sharp transition would greatly enhance the halo formation.

V. EFFECTS OF NONZERO ANGULAR MOMENTUM

We have discussed halo formation for particles with zero angular momentum in Sec. III. It would be interesting to know what the effect of nonzero angular momentum on particle motion is. Using the normalized coordinates of Eq. (20) and the generating function of Eq. (18), the Hamiltonian for a test particle in the KV beam in a paraxial symmetric uniform focusing channel can be expressed as $H_p = H_{p0} + \Delta H_p$, where

$$H_{p0} = \frac{1}{4\pi}p_r^2 + V_{p0}(r, p_\varphi), \tag{59}$$

$$\Delta H = -\frac{K}{2\pi R_0^2}\left[\frac{Y}{R_0}(r^2 - R_0^2) + \cdots\right]\Theta(R_0 - r) \tag{60}$$

are, respectively, the unperturbed Hamiltonian and the perturbation. The unperturbed potential is given by

$$V_{p0}(r, p_\varphi) = \frac{p_\varphi^2}{4\pi r^2} + \pi\nu_y^2 r^2 + \frac{K}{4\pi}\left[\frac{r^2}{R_0^2} - \left(1 + 2\ln\frac{r}{R_0}\right)\right] \times\Theta(r - R_0). \tag{61}$$

Here $(r, p_r, \varphi, p_\varphi)$ are conjugate phase space coordinates. Since the Hamiltonian is independent of φ, the angular momentum p_φ is invariant for any test particle in the KV Hamiltonian.

The unperturbed Hamiltonian is independent of the time variable, therefore, the "energy" is a constant of motion. We now define the radial action J_r for a Hamiltonian torus with a given energy E_p and angular momentum p_φ as

$$J_r = \frac{1}{2\pi}\oint p_r(E_p, r, p_\varphi)dr. \tag{62}$$

Conversely, the energy E_p can be expressed as a function of the action J_r. The radial tune becomes

$$Q_r = \frac{\partial E_p}{\partial J_r}. \tag{63}$$

Using the generating function

$$F(r, J_r, p_\varphi) = \int_{\hat{r}}^{r} p_r(E_p(J_r), r, p_\varphi)dr, \tag{64}$$

where $\hat{r}$ is the maximum radial amplitude of the Hamiltonian torus, we obtain the conjugate angle variable ψ_r as

$$\psi_r = \partial F/\partial J_r. \tag{65}$$

The perturbation can then be expanded in action-angle variables. Since the particle motion inside the KV envelope is linear, the perturbation does not destroy the linear invariant tori of any test particle inside the KV envelope. On the other hand, the Coulomb potential is nonlinear for particles outside the KV envelope radius. Coherent perturbation can result in parametric resonances at stationary phase conditions,

$$n_r\dot{\psi}_r \approx m_r\nu_e. \tag{66}$$

This is the n_r:m_r radial mode parametric resonance. Because the radial amplitude oscillates twice as fast as compared with betatron oscillations in a single plane, the n_r:m_r radial resonance is equivalent to the n:m resonance of Sec. III B 1 with $n = 2n_r$ and $m = m_r$. Parametric resonances and global chaos can be studied similar to that of Sec. III C.

A. Properties of KV particles

First, we examine dynamical properties of the KV core particles. The KV distribution corresponds to particles located on the emittance shell (also the energy shell for a uniform focusing channel) of the four-dimensional phase space (x, p_x, z, p_z). This leads to a uniform distribution in a circle with radius R_0 in the coordinate spaces (x, z). Thus the Coulomb force is also linear inside the envelope radius. In terms of the action variables of Eq. (27), a KV particle satisfies the relation

$$J_{x\mathrm{KV}} + J_{z\mathrm{KV}} = \tfrac{1}{2}, \tag{67}$$

i.e., KV particles are uniformly distributed on a line in the action space. A test particle can be located at any position on the (J_x, J_z) plane of the action space. A beam with dominant KV particles is called a KV beam. If the amplitude of the betatron oscillations of a particle is smaller than the KV radius, the Hamiltonian for the particle is given by

$$H_{pi} = \frac{1}{4\pi}\left(p_r^2 + \frac{p_\varphi^2}{r^2}\right) + \pi\nu_y^2 r^2 \quad (r \le R_0), \tag{68}$$

where the subscript i signifies the Hamiltonian inside the envelope radius.

Since the motion of a particle inside the envelope radius is linear, the particle tune is independent of the amplitude of oscillations, i.e.,

$$E_{pi} = 2\nu_y J_r + \nu_y|p_\varphi|, \tag{69}$$

where the radial tune of the particle is twice that of the particle tune in a single plane (see also Appendix D). From Eq. (69), we obtain

$$2J_{r,\mathrm{KV}} + |p_{\varphi,\mathrm{KV}}| = \tfrac{1}{2} \tag{70}$$

where the subscript KV stands for KV particles. Thus the KV particles are uniformly distributed on a line in the radial action and angular momentum plane. The minimum radial action is zero, thus the maximum angular momentum of KV particles is $\hat{p}_{\varphi,\mathrm{KV}} = 1/2$ (see also Ref. [14]). Similarly, the maximum radial action of KV particles is 1/4.

A test particle inside the envelope core can however be a non-KV particle, which executes linear betatron oscillations. The maximum radial action for a particle executing linear betatron oscillations is given by

$$\hat{J}_{r,c} = \tfrac{1}{2}(|p_\varphi| - 1)^2. \tag{71}$$

Thus a test particle having $J_r \le \hat{J}_{r,c}$ and $|p_\varphi| \le 1$ executes linear betatron oscillations inside the core. It may not be KV particles and yet the perturbation due to envelope oscillations cannot destroy the Hamiltonian torus of this non-KV particle. Only non-KV particles lying outside the envelope core can be perturbed by the envelope oscillations.

B. Properties of particle motion with a nonzero angular momentum

The radial potential V_r for a test particle with a nonzero angular momentum p_φ has a minimum at the radius r_0, where

$$\frac{r_0^2}{R_0^2} = \begin{cases} |p_\varphi|, & \text{if } |p_\varphi| \le 1, \\ \left(\sqrt{\kappa^2 + p_\varphi^2} + \kappa\right)/(\sqrt{\kappa^2+1} + \kappa), & \text{if } |p_\varphi| > 1. \end{cases} \tag{72}$$

Finding the local curvature of the potential around $r = r_0$, one can obtain the tune of small amplitude oscillations. The ratio of the small amplitude tune to the envelope tune becomes

$$\frac{Q_{r0}}{\nu_e} = \begin{cases} \left(1 - \frac{\kappa}{\sqrt{\kappa^2+1}}\right)^{1/2}, & \text{if } |p_\varphi| < 1 \\ \left(\frac{\sqrt{\kappa^2+1}+\kappa}{\sqrt{\kappa^2+1}}\,\frac{\sqrt{\kappa^2+p_\varphi^2}}{\sqrt{\kappa^2+p_\varphi^2}+\kappa}\right)^{1/2}, & \text{if } |p_\varphi| > 1. \end{cases} \tag{73}$$

In particular, we note that the radial tune is discontinuous at $|p_\varphi| = 1$, i.e., $Q_{r0}/\nu_e < 1$ for $|p_\varphi| < 1$, and $Q_{r0}/\nu_e > 1$ for $|p_\varphi| > 1$. This is due to the intrinsic property of the KV model, where the second order derivative of the particle potential is discontinuous across the envelope radius.

The lower plot of Fig. 13 shows Q_r/ν_e vs $\hat{r}/R_0$, where $\hat{r}$ is the maximum radius for a torus of the Hamiltonian flow, with $\kappa = 2$ and angular momenta $p_\varphi = 0.65$, 1.25, and 2.3, respectively. The feature of the radial tune can be understood easily as follows. Since the Hamiltonian is linear for $r \le R_0$, the small amplitude radial tune for a particle with $|p_\varphi| \le 1$ is equal to $2\nu_y$. The radial tune shown in Fig. 13 for the cases $p_\varphi = 0.65$ resembles that

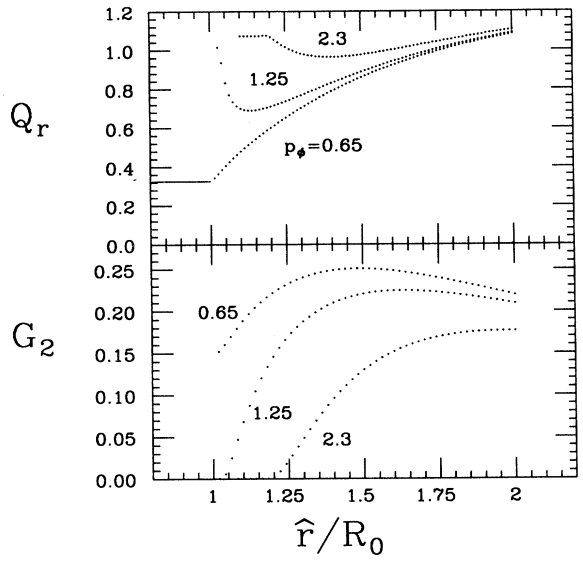

FIG. 13. The upper plot shows Q_r/ν_e vs $\hat{r}$, where $\hat{r}$ is the maximum radial amplitude of a Hamiltonian torus, with $\kappa = 2$ and angular momenta $p_\varphi = 0.65$, 1.25 and 2.3, respectively. For $p_\varphi \leq 1$, the particle tune is nearly independent of angular momentum. The lower plot shows the corresponding strength function G_2 vs $\hat{r}$.

of Fig. 4 with $p_\varphi = 0$. On the other hand, the small amplitude radial tune is larger than ν_e [see Eq. (73)] for $|p_\varphi| > 1$. When the amplitude of the radial motion increases from r_0 with energy $E > \frac{1}{2}\nu_y(1 + p_\varphi^2)$, which is the potential energy at the envelope core, the particle orbit enters the KV core and experiences space charge force and, therefore, the radial tune decreases. As the radial amplitude becomes large, e.g., $\hat{r} > 2R_0$, where the particle orbit stays mostly outside the envelope core, the effect of space charge becomes not important, and the particle radial tune approaches $2\mu/2\pi$. The radial tunes for $p_\varphi = 1.25$ and 2.3 in Fig. 13 display this characteristic clearly. Appendix D provides an approximate solution by employing a superposition of linear solutions in two different regions in order to simulate the nonlinear detuning arising from the Coulomb potential.

Note here that the radial tune of a test particle is nearly independent of the angular momentum for $\hat{r} > 1.5R_0$. On the other hand, the radial tune of a particle with angular momentum $p_\varphi > 1$ can satisfy a parametric resonance condition at two regions of phase space. For example, there are two phase space trajectories that satisfy the radial 1:1 resonance condition for $p_\varphi = 2.3$ (see Fig. 13). The bifurcation of these resonances is similar to that of a double rf system [15]. The resonance strengths for these resonances are generally very small because their trajectories enter the core only slightly. Nevertheless, local chaos can be created when the resonance overlapping condition is satisfied. Beyond $\hat{r} > 1.5R_0$, the radial tune is nearly identical for particles with different angular momenta, thus the single plane 2:1 resonance condition of Sec. III B 1, which is equivalent to the radial 1:1 resonance, is relatively independent of the angular momenta of test particles.

The resonance strength function of Eq. (39) for G_2 is shown in the lower plot of Fig. 13 for $\kappa = 2$ with $p_\varphi = 0.65$, 1.25, and 2.3, respectively. Since the radial 1:1 resonance strength function for different angular momentum at the resonance location $\hat{r} \approx 1.8R_0$ decreases slightly with increasing angular momentum, the width of the resonance decreases also slightly with angular momentum.

C. Effects of angular momentum on halo formation

To study the effects of the KV envelope oscillations on particle motion with angular momentum, we study the Hamiltonian dynamics of Eqs. (59) and (60) with $Y/R_0 = M\cos\nu_e\theta$, which approximate the coupled KV and Hill's equations. In this 1D model of radial oscillations, the Poincaré surface of section can be obtained by plotting phase space points at a time interval of $\Delta\theta = 2\pi/\nu_e$. The radial tunes for $\kappa = 2$ and $p_\varphi = 0.65$, 1.25, and 2.3 are shown in Fig. 13. Because the radial tune is relatively independent of the angular momentum of a particle with $|p_\varphi| \leq 1$, conditions and phase space locations of parametric resonances are also independent of the angular momentum. Chaos and halo formation can be analyzed in a similar fashion as that of particles with zero angular momentum (see Sec. III). The upper plot of Fig. 14 shows the Poincaré surfaces of section in (p_r, r) phase space for $\kappa = 2$ and $p_\varphi = 0.65$ (see Fig. 13) with the modulation amplitude $M = 0.04$.

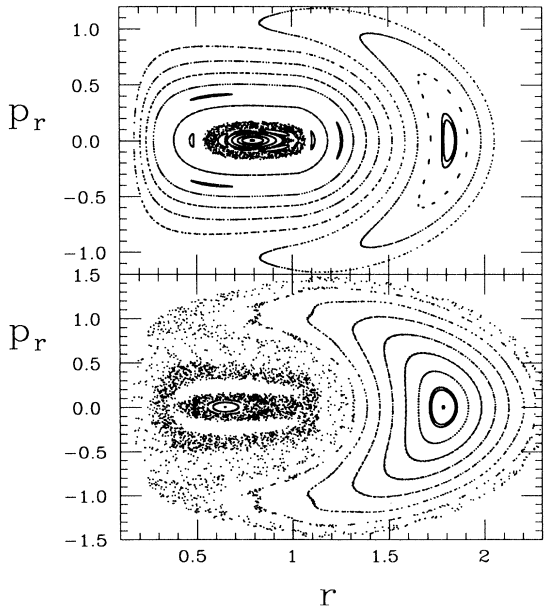

FIG. 14. The radial Poincaré surfaces of section in (p_r, r) with $\kappa = 2, p_\varphi = 0.65$. The upper plot, with $M = 0.04$, exhibits the primary and the secondary resonances. The lower plot at $M = 0.16$ displays global chaos resulting from overlapping resonances.

Note particularly that the primary radial modes, 1:1, 2:1, and 3:1 are clearly visible. The secondary 3:2 resonance resulting from the combination of the 1:1 and 2:1 primary resonances is clearly visible at this small modulation amplitude. The local chaos around the envelope core presumably arises from the overlapping secondary 5:2 resonance with the primary 3:1 resonance. A global chaos can also result from the overlapping radial 1:1 resonance and the local chaos near the envelope core. For example, global chaos appears in the lower plot of Fig. 14 where $M = 0.16$ is used in our simulation. This is to be compared with that of Fig. 10, where there is no global chaos for $\kappa = 2$ until $M \gg 0.4$.

The radial tune of a particle with angular momentum $|p_\varphi| > 1$ exhibits a minimum as a function of $\hat{r}$ (see Fig. 13). This implies that there are two separate radial orbits, which can satisfy the resonance condition, $nQ_r(\hat{r}) \approx m\nu_e$, for the radial n:m resonance. Figure 15 shows the radial Poincaré surfaces of section for $\kappa = 2$ and $p_\varphi = 2.3$ with $M = 0.04$ (upper) and 0.16 (lower), respectively. For $M = 0.04$, we observe two 1:1 resonances that correspond to $Q_r/\nu_e = 1$. The third SFP corresponds to the minimum of the radial potential of Eq. (61). When the modulation amplitude is increased to $M = 0.16$, the inner 1:1 resonance has bifurcated. The reminiscence of the 1:1 resonance remains visible.

For particles with angular momentum slightly larger than one, the radial tune decreases very fast near $\hat{r} \approx R_0$ (see Fig. 13), the radial parametric resonances are more densely packed in the radial phase space (p_r, r). Local

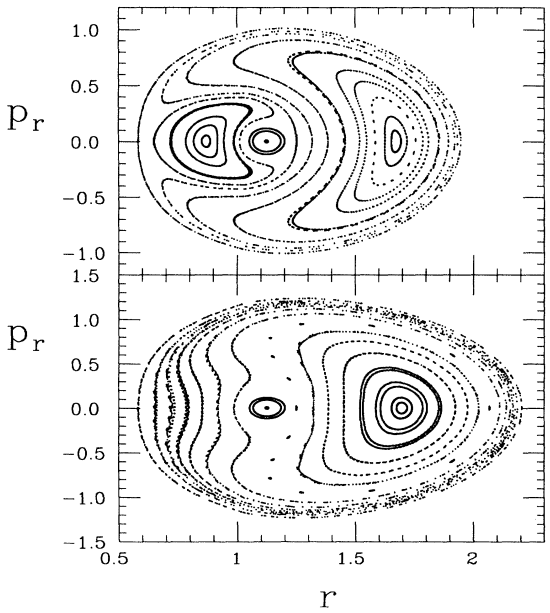

FIG. 15. The Poincaré surfaces of section $\kappa = 2, p_\varphi = 2.3$ for $M = 0.04$ (upper) and 0.16 (lower), respectively. For $M = 0.04$, there are two 1:1 resonances in accordance with the radial tune shown in Fig. 13. When the modulation amplitude is increased, higher order perturbation can become important to cause the inner 1:1 resonance to bifurcate.

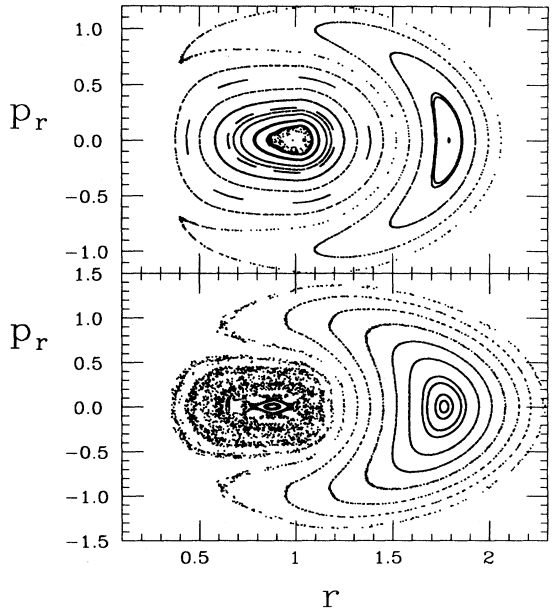

FIG. 16. The Poincaré surfaces of section $\kappa = 2, p_\varphi = 1.25$ for $M = 0.04$ (upper) and 0.16 (lower), respectively. The inner 1:1 resonance is too weak to be visible for $M = 0.04$. When the modulation amplitude is increased, higher order resonances cause local chaos near the envelope core.

chaos can result from a smaller perturbation due to envelope oscillations. In fact, because the perturbation due to envelope oscillations is relatively large, overlapping higher order parametric resonances are the main reason of local chaos. Figure 16 shows radial Poincaré surfaces of section with parameters $\kappa = 2, p_\varphi = 1.25$ for $M = 0.04$ (upper) and $M = 0.16$ (lower), respectively.

When the angular momentum becomes very large, e.g., $p_\varphi \geq p_{\varphi c}$, where $p_{\varphi c} \approx 2.5$ for $\kappa = 2$, the radial tune would never cross the radial 1:1 resonance. Does this mean that the halo is complete suppressed? The answer is yes and no. For the case that $p_\varphi \gg p_{\varphi c}$, where $p_{\varphi c}$ is the critical angular momentum, then the halo is completely suppressed. However, when p_φ is just above $p_{\varphi c}$, the halo can be generated by the second order perturbation. This means that a large envelope modulation can produce a nonlinear detuning through the second order canonical perturbation. In this process, the radial 1:1 resonance (halo) can exist. Numerical simulations indeed support this observation. Nevertheless, we can conclude that particles with large angular momenta are less susceptible to envelope oscillations. If one can create a dominant KV beam with non-KV particles having large angular momenta, then the beam transport is less prone to halo formation.

VI. CONCLUSION

In conclusion, the beam transport problem is studied in a one-way self-consistency model by solving the KV

envelope and Hill's equations in Hamiltonian dynamics. Parametric resonances of the particle Hamiltonian can be generated by a mismatched envelope oscillations. The resonance condition is found to depend only on a single effective space charge parameter κ, i.e., the ratio of the space charge perveance parameter to the phase advance of the focusing field. Due to the mismatched beam envelope oscillations, the 2:1 resonance occurs at all space charge perveance parameters.

Our theoretical analysis agrees well with numerical simulations. We prove analytically that the linear Mathieu resonance plays no role in the halo formation, where halo particles are defined as particles that orbit the 2:1 resonance islands. Using our approach, the condition for the halo formation is derived based on the existence of tail particles outside the artificial KV envelope function.

From our numerical simulations, the critical Poincaré energy for the halo particle exhibits a first order phase-transition-like behavior when plotted as a function of the envelope mismatch parameter. This first order phase-transition-like behavior can be unambiguously identified as the onset of global chaos. The relation between the critical mismatch parameter M_c and the effective space charge parameter κ is obtained from numerical simulations. Effects of global chaos on halo formation are discussed. Effects of angular momentum on halo formation are examined, and some experimental tests of the theoretical model are suggested. These experiments are important to confirm the validity of the space charge model by studying the KV and Hill's equations.

In this paper, we have studied only the halo formation for space charge dominated beams in a uniform focusing channel. This method can readily be applied to study the beam transport problems in a solenoidal periodic focusing channel and the quadrupole focusing channel, where Floquet transformation is needed before analytic solution can be obtained. Extension of the present work is highly desirable for future studies.

ACKNOWLEDGMENTS

Work supported in part by NSF Grant No. PHY-9221402 and the DOE Grant No. DE-FG02-93ER40801. We thank C.L. Bohn, R.L. Gluckstern, and R.A. Jameson for several helpful comments.

APPENDIX A: SYMMETRY PROPERTIES OF THE HAMILTONIANS

Making a scaling transformation: $\tilde{\theta} = \mu\theta$ for the time coordinate, $(\tilde{y}, \tilde{p}) = (\sqrt{\mu}y, \frac{p}{\sqrt{\mu}})$ for the conjugate particle phase space variables, and $(\tilde{R}, \tilde{P}) = (\sqrt{\mu}R, \frac{P}{\sqrt{\mu}})$ for the conjugate envelope phase space variables, the new envelope and particle Hamiltonians becomes

$$\tilde{H}_e = \frac{1}{4\pi}\tilde{P}^2 + \frac{1}{4\pi}\tilde{R}^2 - \frac{\kappa}{\pi}\ln\tilde{R} + \frac{1}{4\pi\tilde{R}^2}, \tag{A1}$$

$$\tilde{H}_p = \frac{1}{4\pi}\tilde{p}^2 + \frac{1}{4\pi}\tilde{y}^2 - \frac{\kappa}{2\pi\tilde{R}^2}\tilde{y}^2\Theta(\tilde{R} - |\tilde{y}|) - \left(\frac{\kappa}{2\pi} + \frac{\kappa}{\pi}\ln\frac{\tilde{y}}{\tilde{R}}\right)\Theta(|\tilde{y}| - \tilde{R}). \tag{A2}$$

Here, the new Hamiltonians depend only on a single space charge parameter $\kappa = K/2\mu$. Thus the KV space charge model in a uniform focusing channel is a single parameter Hamiltonian system.

APPENDIX B: THE SPACE CHARGE FORCE

Within the KV equilibrium envelope model, test particles obey Hamilton's equations of motion (23). The space charge force experienced by test particles has a cusp at $y = R$, i.e., $F_{sp} = F_1(y)\Theta(R - |y|) + F_2(y)\Theta(|y| - R)$, where $F_1(y)$ and $F_2(y)$ can be obtained easily from Eq. (23). The Θ function is very unfriendly in the perturbation treatment. However, we can make a successive averaging approximation to the space charge force with

$$\frac{1}{F_{sp1}(y)} = \frac{1}{F_1(y)} + \frac{1}{F_2(y)}. \tag{B1}$$

The space charge force can now be written as

$$F_{sp} = F_{sp1} + \Delta F_1\Theta(R - |y|) + \Delta F_2\Theta(|y| - R). \tag{B2}$$

The averaging procedure can be performed iteratively on the remainder force $\Delta F_1, \Delta F_2$. This successive averaging procedure converges rapidly. The model presented in Eqs. (24) and (26) agrees well with the limiting case of the averaging procedure.

APPENDIX C: NUMERICAL SIMULATIONS

Numerical results are obtained by solving Hamilton's equations of motion for the envelope and particle Hamiltonians simultaneously, i.e.,

$$\ddot{R} + \left(\frac{1}{2\pi}\right)^2\left[\mu^2 R - \frac{K}{R} - \frac{1}{R^3}\right] = 0, \tag{C1}$$

$$\ddot{y} + \left(\frac{1}{2\pi}\right)^2\left[\mu^2 y - \frac{K}{R^2}y\Theta(R - |y|) - \frac{K}{y}\Theta(|y| - R)\right] = 0. \tag{C2}$$

We use a fourth order symplectic integrator to solve these one-way coupled second order differential equations to obtain the phase space maps. The Poincaré surface of section is obtained by plotting one particle phase space point whenever the envelope phase space recurs. The Poincaré surface of section effectively removes uninteresting time dependent component of phase space maps while retaining dynamic resonances. The result is equivalent to the resonance rotating frame discussed in Sec. III B.

The Poincaré surfaces of section shown in Figs. 6–9 and 12 correspond actually to the phase space map of p_b vs y_b. The parameters are chosen as $K_b = 1$, $\mu_f = 1$, while the emittance ϵ is varied to obtain a proper space charge parameter $\kappa = K_b/2\mu_f\epsilon$. The phase space area of

the envelope ellipse is proportional to $\sqrt{\epsilon}$. This choice of parameter will maintain the Poincaré surfaces of section having nearly identical radius. This is evident that $R_0 = R_b$ is almost identical for all cases.

APPENDIX D: AN APPROXIMATE SOLUTION TO PARTICLE MOTION WITH ANGULAR MOMENTUM

Although Gluckstern (see Eqs. (2.11)–(2.16) of Ref. [14]) obtained analytic solution by employing Bogoliubov averaging method on the Coulomb potential, his result did not give rise to a cusp in the particle tune around $\hat{r} = R_0$. Since the cusp in the particle tune is important in producing local chaos due to higher resonances, we would like to explore an alternative approximation scheme, which can provide us a better representation of the particle tune.

Let the Hamiltonian H_{p0} of Eq. (59) be approximated by H_{pa} with

$$H_{pa} = \frac{1}{4\pi}\left(p_r^2 + \frac{p_\varphi^2}{r^2}\right) + \pi\nu_y^2 r^2 + \frac{1}{4\pi}\left[A + Br^2 + \frac{C}{r^2}\right]\Theta(r - R_0), \tag{D1}$$

where two of the parameters A, B, and C can be determined by the continuity conditions at $r = R_0$, i.e., $A = -2C/R_0^2$ and $B = C/R_0^4$. The remaining parameter C can be best adjusted to obtain a proper particle tune near the resonance region.

In this model, the minimum radius position of the potential well is given by

$$\frac{r_0^2}{R_0^2} = \begin{cases} |p_\varphi|, & \text{if } |p_\varphi| \le 1, \\ \frac{\sqrt{p_\varphi^2 + C}}{\sqrt{1+C}}, & \text{if } |p_\varphi| > 1, \end{cases} \tag{D2}$$

which agrees reasonably well with that of Eq. (72) provided that C is properly chosen. The corresponding minimum energy is

$$E_0 = \begin{cases} \nu_y |p_\varphi|, & \text{if } |p_\varphi| \le 1, \\ \nu_y \left[\sqrt{(1+C)(p_\varphi^2 + C)} - C\right], & \text{if } |p_\varphi| > 1. \end{cases} \tag{D3}$$

For a given energy, the solutions for the approximate Hamiltonian H_{pa} are given by

$$\frac{r^2}{R_0^2} = \begin{cases} \frac{E}{\nu_y} + \sqrt{E^2/\nu_y^2 - p_\varphi^2}\cos(2\nu_y\theta + \chi_i) & (r \le R_0), \\ \frac{E/\nu_y + C}{1+C} + \frac{\sqrt{(E/\nu_y + C)^2 - (1+C)(p_\varphi^2 + C)}}{1+C}\cos(2\nu_y\sqrt{1+C}\theta + \chi_o) & (r > R_0), \end{cases} \tag{D4}$$

for the particle inside and outside the envelope radius, respectively. A solution to the approximate Hamiltonian is then obtained by matching the inner and outer solutions at $r = R_0$. A trajectory inside the envelope radius will have a radial tune $2\nu_y$ and a trajectory outside has a radial tune of $2\nu_y\sqrt{1+C}$. A trajectory with mixed inner and outer paths will have a tune determined by a proper matching condition. The parameter C can be chosen to best fit the particle tune near the important resonance region. We thus approximate the detuning due to the nonlinear Coulomb potential by varying components of two linear oscillations.

Using Hamilton's equation of motion, the radial tune Q_r of a Hamiltonian torus is given by

$$Q_r = \begin{cases} 2\nu_y, & \text{if } E \le 0.5\nu_y(1 + p_\varphi^2), \\ 1/(N_o + N_i), & \text{if } E > 0.5\nu_y(1 + p_\varphi^2), \end{cases} \tag{D5}$$

where

$$N_o = \frac{1}{2\pi\nu_y\sqrt{1+C}} \times \arccos\frac{-(E - \nu_y)}{\sqrt{(E + C\nu_y)^2 - \nu_y^2(1+C)(p_\varphi^2 + C)}},$$
$$N_i = \frac{1}{2\pi\nu_y}\arccos\frac{E - \nu_y}{\sqrt{E^2 - \nu_y^2 p_\varphi^2}}, \tag{D6}$$

are, respectively, the number of periods that the particle stays outside and inside the envelope core in one complete radial oscillation. For a given energy E, the maximum radial amplitude of the torus can be obtained from Eq. (D4). The asymptotic radial tune at $E \to \infty$ is $Q_r \to 2\nu_y\sqrt{1+C}$. A satisfactory choice of the parameter C from our numerical calculations is $C \approx 2d\kappa/(\sqrt{\kappa^2 + 1} - \kappa)$, which simulates the particle tune reasonably well in the region of $\hat{r}/R_0 \in [1, 2.5)$. The choice of this parameter gives the following asymptotic property:

$$Q_r\big|_{\hat{r}\to\infty} \to 2\nu_y\sqrt{1+C} \approx 2\sqrt{d}\frac{\mu}{2\pi}. \tag{D7}$$

Our numerical simulations show that $d \approx 0.65$–0.7 provides satisfactory approximation to the nonlinear detuning. The choice deviates from the exact asymptotic value of $2(\mu/2\pi)$ by 14–20 %. The resonance strength function, obtained analytically by using the approximate solutions, agrees also reasonably well with the exact solutions.

[1] J.D. Lawson, *Physics of Charged Particle Beams*, 2nd ed. (Oxford University Press, New York, 1988); R.C. Davidson, *Physics of Nonneutral Plasma* (Addison-Wesley, Reading, MA, 1990); A.W. Chao, *Physics of Collective Instabilities in High Energy Accelerators* (J. Wiley & Sons, Inc., New York, 1993).

[2] R.A. Jameson, *Proceedings of the 1993 Particle Accelerator Conference* (IEEE, Piscataway, 1993), p. 3926; (unpublished).

[3] I.M. Kapchinskij and V.V. Vladimirskij, in *Proceedings of the 9th International Conference on High Energy Accelerators*, edited by L. Kowarski (CERN, Geneva, 1959), p. 274.

[4] P.M. Lapostolle, IEEE Trans. Nucl. Sci. **NS-18**, 1101 (1971); F.J. Sacherer, *ibid.* **N5-18**, 1105 (1971); J.D. Lawson, P.M. Lapostolle, and R.L. Gluckstern, Part. Accel. **5**, 61 (1973); E.P. Lee and R.K. Cooper, *ibid.* **7**, 83 (1976).

[5] C. Chen and R.C. Davidson, Phys. Rev. E **49**, 5679 (1994); Phys. Rev. Lett. **72**, 2195 (1994).

[6] S.Y. Lee and A. Riabko, Phys. Rev. E **51**, 1609 (1995).

[7] J.S. O'Connell, T.P. Wangler, R.S. Mills, and K.R. Crandall, in *Proceedings of the Particle Accelerator Conference*, edited by J. Bisognano (IEEE, Piscataway, NJ, 1993), p. 3657.

[8] J.M. Lagniel, Nucl. Instrum. Methods Phys. Res. **A345**, 46 (1994); **A345**, 405 (1994).

[9] I. Hofmann, L.J. Laslett, L. Smith, and I. Haber, Part. Accel. **13**, 145 (1983); J. Struckmeier and M. Reiser, Part. Accel. **14**, 227 (1983).

[10] T.P. Wangler, K.R. Crandall, R.S. Mills, and M. Reiser, IEEE Trans. Nucl. Sci. **32**, 2196 (1985); M. Reiser, *ibid.* **32**, 2201 (1985).

[11] I. Haber *et al.*, Phys. Rev. A **44**, 5194 (1991); M. Reiser, J. Appl. Phys. **70**, 1919 (1991); D. Kehne *et al.*, in *Proceedings of the Particle Accelerator Conference* (Ref. [7]), p. 65.

[12] J.A. Palkovic, in *Proceedings of the Particle Accelerator Conference* (Ref. [7]), p. 21.

[13] C.L. Bohn, Phys. Rev. Lett. **70**, 932 (1993); C. L. Bohn and J. R. Delayen, Phys. Rev. E **50**, 1516 (1994); C. L. Bohn and J. R. Delayen, in *Proceedings of the Particle Accelerator Conference*, edited by J. Bisognano (IEEE, Piscataway, NJ, 1993), p. 3666.

[14] R.L. Gluckstern, Phys. Rev. Lett. **73**, 1247 (1994).

[15] S.Y. Lee *et al.*, Phys. Rev. E **49**, 5717 (1994).

[16] M. Ellison *et al.*, Phys. Rev. Lett. **70**, 591 (1993); H. Huang *et al.*, Phys. Rev. E **48**, 4678 (1993); D. Li *et al.*, *ibid.* **48**, R1638 (1993); M. Syphers *et al.*, Phys. Rev. Lett. **71**, 719 (1993); Y. Wang *et al.*, Phys. Rev. E **49**, 1610 (1994).

[17] One can choose equally well the maximum envelope radius locations for the particle Poincaré surfaces of section. The physics remains the same.

[18] S. Machida, in *Proceedings of the Particle Accelerator Conference* (Ref. [7]), p. 3224.

[19] S.K. Guharay *et al.*, Rev. Sci. Instrum. **65**, 1774 (1994).